

Free-floating planets from core accretion theory: microlensing predictions

Sizheng Ma¹, Shude Mao^{1,2,3*}, Shigeru Ida⁴, Wei Zhu⁵, Douglas N.C. Lin^{1,2,6}

¹ Department of Physics and Center for Astrophysics, Tsinghua University, Haidian District, Beijing 100084, China

² National Astronomical Observatories, 20A Datun Road, Chinese Academy of Sciences, Beijing, 100012, China

³ Jodrell Bank Centre for Astrophysics, School of Physics and Astronomy, University of Manchester, Alan Turing Building, Oxford Road, Manchester M13 9PL, UK

⁴ Earth-Life Science Institute, Tokyo Institute of Technology, Okayama, Meguro-ku, Tokyo 152-8550, Japan

⁵ Department of Astronomy, The Ohio State University, 140 W. 18th Avenue, Columbus, OH 43210, USA

⁶ University of California Observatories, Lick Observatory, University of California, Santa Cruz, CA 95064

Accepted Received ; in original form.....

ABSTRACT

We calculate the microlensing event rate and typical time-scales for the free-floating planet (FFP) population that is predicted by the core accretion theory of planet formation. The event rate is found to be $\sim 1.8 \times 10^{-3}$ of that for the stellar population. While the stellar microlensing event time-scale peaks at around 20 days, the median time-scale for FFP events (~ 0.1 day) is much shorter. Our values for the event rate and the median time-scale are significantly smaller than those required to explain the Sumi et al. (2011) result, by factors of ~ 13 and ~ 16 , respectively. The inclusion of planets at wide separations does not change the results significantly. This discrepancy may be too significant for standard versions of both the core accretion theory and the gravitational instability model to explain satisfactorily. Therefore, either a modification to the planet formation theory is required, or other explanations to the excess of short-time-scale microlensing events are needed. Our predictions can be tested by ongoing microlensing experiment such as KMTNet, and by future satellite missions such as WFIRST and Euclid.

Key words: planets and satellites: detection, formation - gravitational lensing: micro - Galaxy: bulge

1 INTRODUCTION

Microlensing as a method to detect planets around a host star was proposed 25 years ago (Mao & Paczynski 1991; Gould & Loeb 1992). So far more than 40 planets discovered by microlensing have been published¹, with many more discovered but yet to be published. Microlensing probes the planet population beyond the snow line in the planet mass vs. host star separation parameter space, and is complementary to other detection methods (see Gaudi 2012; Mao 2012 for reviews).

A significant advantage of the microlensing method is that it can detect free-floating planets (FFPs). Events caused by FFPs have short time-scales because time-scales scale as $M^{1/2}$, where M is the lens mass (cf. eq. 1). For example, the typical time-scale is of order 1 day for a Jupiter-mass FFP and a few hours for an Earth-mass FFP.

Ground-based high-cadence surveys, such as the Microlensing Observations in Astrophysics (MOA-II; Bond et al. 2001; Sumi et al. 2003), the Optical Gravitational Lensing Experiment (OGLE-IV; Udalski, Szymański & Szymański 2015), and now the Korean Microlensing Telescope Network (KMTNet, Kim et al. 2016; Hendersson et al. 2014), are in principle able to detect such events.

The MOA-II collaboration in fact detected 10 events with an Einstein radius crossing time-scale $t_E < 2$ days among 474 well characterized events in their 2006–2007 data set. After correcting the detection efficiency, Sumi et al. (2011) concluded that a population of unbound or distant Jupiter-mass objects that are almost twice as common as stellar objects is required to explain the observed time-scale distribution.

An immediate question is whether the result in Sumi et al. (2011) is consistent with predictions from planet formation models. The two competing theories of planet formation are core accretion (e.g., Ida & Lin 2004; Mordasini, Alibert & Benz 2009; Ida, Lin & Nagasawa

* smao@tsinghua.edu.cn

¹ <http://exoplanet.eu>

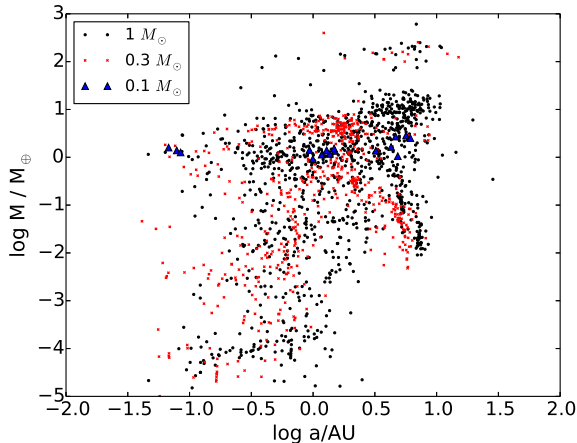


Figure 1. The mass and semi-major axis (before ejection) distributions of the FFP populations used in this work. The three different symbols are used for FFPs ejected from three different host star masses (1, 0.3, and 0.1 M_{\odot}). In total 1000 planetary systems have been simulated, with 1069, 571 and 17 ejected planets, respectively.

2013) and gravitational instability (e.g., Boss 2006). In this paper, we focus on the former, but also address the influence of the latter in Section 6. Population synthesis models in the core accretion regime have taken into account many physical processes (such as migration and collision), and can provide detailed predictions about the properties of not only the bound planet population (Ida & Lin 2004; Mordasini et al. 2009) but also FFPs. These FFPs are formed inside the proto-planetary disk and ejected due to dynamical interactions with other objects (see also Pfyffer et al. 2015).

The purpose of this work is to study the microlensing signature of the FFP population predicted by the popular core accretion theory. The structure of this paper is as follows: in §2, we review the properties of the FFP population as predicted by Ida, Lin & Nagasawa (2013); in §3 and §4, we describe microlensing basics and the simple Galactic model that we use for creating microlensing observables from our FFP populations; our results are presented in §5; and finally in §6, we summarise and discuss our work.

2 PROPERTIES OF THE FFP POPULATIONS

We adopt the planet population synthesis model that is described in Ida, Lin & Nagasawa (2013). Note that their simulations have different parameter settings, for example regarding the orbital migration of planets, which may lead to slight differences in the ejected planets' population. In this work, we use the results from their most up-dated simulations, in which the planet migrations are described as non-isothermal processes. Readers can find the distributions of the bound planet population predicted by such simulations in Fig. 14 of Ida, Lin & Nagasawa (2013). Their calculation starts from very small planetary seeds; planets with mass larger than $1 \times 10^{-5} M_{\oplus}$ have already increased their masses significantly and are thus not affected by initial conditions.

Their results for three host star masses, $1M_{\odot}$, $0.3M_{\odot}$

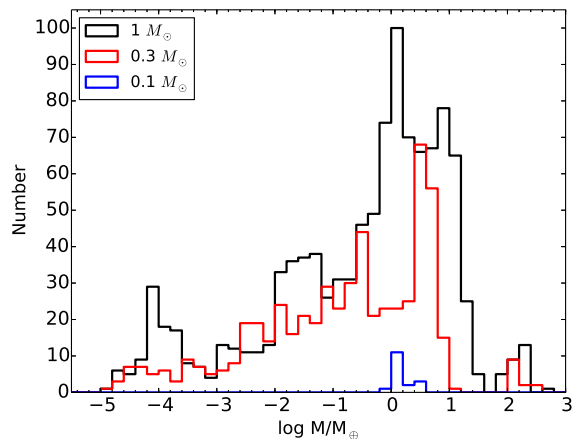


Figure 2. The mass function of the free-floating planets. The three lines are for three host star masses, i.e., 1, 0.3 and $0.1M_{\odot}$ respectively.

Table 1. Summary of the FFP populations used in this work. The last column indicates the fraction of stellar systems with ejected planets; the third column indicates the mean and median masses of individual ejected planets for each stellar mass; the fourth column indicates those of the total planetary mass ejected from individual system. All the planetary masses are in units of M_{\oplus} .

M_{\star}		Individual FFP mass (M_{\oplus})	Total FFP mass (M_{\oplus})	Fraction
$1 M_{\odot}$	mean	7.2	44.2	17.5 %
	median	0.8	16.8	
$0.3 M_{\odot}$	mean	5.2	24.5	12 %
	median	0.3	5.1	
$0.1 M_{\odot}$	mean	1.6	3.3	0.8 %
	median	1.4	3.0	

and $0.1M_{\odot}$, are used here. For each stellar mass, 1000 systems are simulated. In total there are respectively 1069, 571 and 17 ejected planets. Fig. 1 shows the ejected planets in the mass vs. semi-major axis plane just before ejection while Figs. 2 and 3 show the histograms of the masses and semi-major axes, respectively. For $0.3M_{\odot}$ and $1M_{\odot}$ stars, one sees an ejected population of Jupiter-mass planets and then more abundant super-Earth planets, followed by an extended tail down to $10^{-5} M_{\oplus}$.

Only a minority of simulated stellar systems produce free-floating planets: for 1, 0.3 and $0.1M_{\odot}$, these fractions are 17.5%, 12% and 0.8%, respectively (see Table 1). The third column of Table 1 shows the mean and median masses of all ejected planets. In each case, the median planet mass is much smaller than the mean due to the extended tail down to very low masses. It is interesting to note that the mean values are only a few Earth masses in all cases.

For systems that eject planets, each system tends to eject more than one planet. This is illustrated in Fig. 4. For 1, 0.3 and $0.1M_{\odot}$ stars, each system on average ejects 6.1, 4.8, and 2.1 planets, respectively. We sum up their total masses and list the mean and median values in the fourth

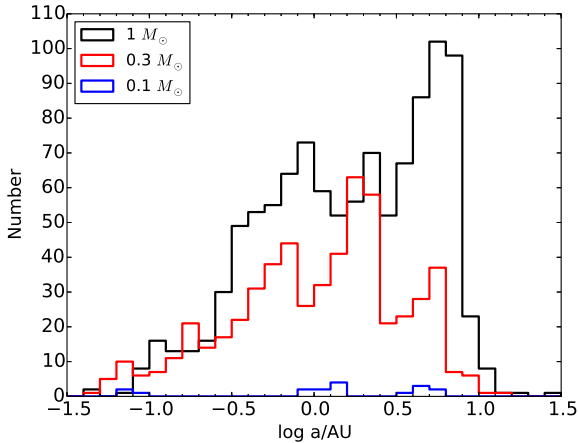


Figure 3. The distribution of the semi-major axis just before the ejection. The symbols are the same as in Fig. 2.

column of Table 1; the mean values of total ejected mass are $24.5M_{\oplus}$ and $44.2M_{\oplus}$ for $0.3M_{\odot}$ and $1M_{\odot}$ stars respectively. For $0.1M_{\odot}$ stars, the value is significantly smaller ($3.3M_{\oplus}$).

The ejected planets are generally scattered by emerging gas giants which have sufficient mass to induce recoil speeds comparable to or larger than their escape velocities. Since gas giants form less frequently around low-mass stars, the ejected fraction from their domain is much lower than that for the FGK stars. Around $1M_{\odot}$ stars, the initial location of the escapers is preferentially outside 1AU (see Figs. 5-3) because 1) the binding energy by the host stars decreases as the separation increases and 2) birth places of the gas giants are preferentially near the snow line. The timescale for forming progenitor cores increases with the semi-major axis. Beyond 10 AU from the host star, the formation probability of gas giant declines. Nonetheless, a few Neptune-mass failed cores may still scatter some residual planetesimals out of the gravitational confines of their host stars.

3 MICROLENSING BASICS

3.1 Event time-scale

The Einstein radius (r_E) crossing time-scale is given by

$$t_E \equiv \frac{r_E}{v_t} \approx 19 \text{ d} \sqrt{4 \times \frac{D_L}{D_S} \left(1 - \frac{D_L}{D_S}\right) \left(\frac{D_S}{8 \text{ kpc}}\right)^{1/2}} \times \left(\frac{M}{0.3M_{\odot}}\right)^{1/2} \left(\frac{v_t}{200 \text{ km s}^{-1}}\right)^{-1}, \quad (1)$$

where D_S and D_L are the distances to the source and the lens, respectively, M is the lens mass and v_t is the transverse velocity (Mao 2012). The time-scale is proportional to $M^{1/2}$; for a $0.3M_{\odot}$ star, it is around 20 days.

3.2 Event rate and optical depth

The optical depth is the probability that a given source falls into the Einstein radius of any lensing star along the line of

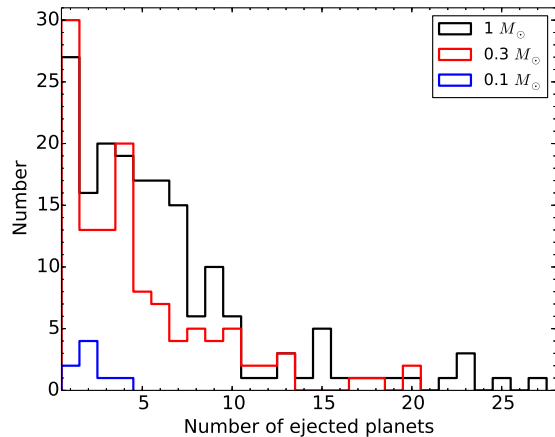


Figure 4. Histogram of the numbers of ejected planets from individual systems.

sight, and is defined as (see, e.g., Paczynski 1996 for reviews)

$$\tau = \int_0^{D_S} n(D_L) (\pi r_E^2) dD_L, \quad (2)$$

where $n(D_L)$ is the number density of lenses. For a source population distributed at various distances, it can be written as (e.g., Kiraga & Paczynski 1994; Wood & Mao 2005)

$$\langle \tau \rangle_{\gamma} = \frac{4\pi G}{c^2} \int_0^{\infty} dD_S D_S^{2-\gamma} \rho(D_S) \int_0^{D_S} dD_L \rho(D_L) D_L \frac{D_S - D_L}{D_S} \times \left[\int_0^{\infty} dD_S D_S^{2-\gamma} \rho(D_S) \right]^{-1}, \quad (3)$$

where $\rho(D_S)$ and $\rho(D_L)$ are the densities of the source and lens at each position, and γ is related to the source luminosity function (we take $\gamma = 0$ as in Wood & Mao 2005).

The event rate (Γ) describes the number of microlensing events per unit time for a given number of monitored stars (N), and is given by

$$\Gamma = \frac{2N}{\pi} \int \frac{d\tau}{t_E}, \quad (4)$$

which can be calculated as

$$\Gamma = \frac{4G^{1/2}}{c} \int_0^{\infty} dD_S D_S^{2-\gamma} \rho(D_S) \times \frac{\int_0^{D_S} dD_L \rho(D_L) v [D_L(D_S - D_L)/MD_S]^{1/2}}{\int_0^{\infty} dD_S D_S^{2-\gamma} \rho(D_S)}. \quad (5)$$

4 GALACTIC MODEL

Given the uncertainties in the planet population synthesis model (see Ida, Lin & Nagasawa 2013), it is sufficient to adopt a simple Galactic model that describes the stellar density and kinematics. We therefore adopt the model used in Wood & Mao (2005) (see also, e.g., Han & Gould 1996; Awiphan, Kerins & Robin 2015).

4.1 Lens and source density distributions

We use the G2 (barred) model (Dwek et al. 1995), with $R_{\max} = 5$ kpc. The distance to the Galactic Centre is taken to be 8 kpc. This is different from the 8.5 kpc value in Dwek et al. (1995), so other lengths are scaled down proportionally. The major axis of the bar is inclined by 30° with respect to the sight-line toward the Galactic Centre, as suggested by several recent studies (Cao et al. 2013; Wegg & Gerhard 2013), instead of 13.4° as adopted in Wood & Mao 2005.

The model requires normalisation to observed star counts and we use HST star counts as in Wood & Mao (2005). In addition, we assume that the stellar mass function is a δ -function at (1, 0.3, 0.1) M_\odot . Correspondingly, each star on average ejects (1.069, 0.571, 0.017) planets, with masses randomly drawn from the distributions shown in Fig. 1. We present the results toward the direction $(l, b) = (1^\circ.50, -2^\circ.68)$ as in Wood & Mao (2005); for other lines of sight, the ratio between the stellar and planetary microlensing events is nearly unchanged.

4.2 Kinematics

We assume that the observer follows the Galactic rotation, so the velocities in the longitudinal and latitudinal directions are given by

$$v_{O,l} = 220 \text{ km s}^{-1}, \quad v_{O,b} = 0 \text{ km s}^{-1}. \quad (6)$$

For rotation of the disc, we use $v_{\text{rot}} = 220$ km/s; for the bar, the v_{rot} is taken to be (Han & Gould 1996)

$$v_{\text{rot}} = v_{\max} \left(\frac{x}{1 \text{ kpc}} \right), \quad R < 1 \text{ kpc}, \quad (7)$$

$$v_{\text{rot}} = v_{\max} \left(\frac{x}{R} \right), \quad R \geq 1 \text{ kpc},$$

where $R = (x^2 + y^2)^{1/2}$ and $v_{\max} = 100 \text{ km s}^{-1}$. The coordinates (x, y, z) have their origin at the Galactic Centre, and the x and z axes point towards the Earth and the North Galactic Pole respectively. In addition to the systematic rotations, stars also have random motions (assumed to be Gaussian). For the disc, the velocity dispersions are taken to be $\sigma_{l,b} = (30, 20) \text{ km s}^{-1}$, and for the bar, $\sigma_{x,y,z} = (110, 82.5, 66.3) \text{ km s}^{-1}$ along the major, intermediate and minor (vertical) axes. These numbers are also the same as Han & Gould (1996). The total velocity for a disc or bar star is a sum of the rotation and local random motions:

$$v_l = v_{\text{rot}} + v_{\text{rand},l} \quad v_b = v_{\text{rand},b}. \quad (8)$$

The transverse velocity, decomposed into two directions, v_l and v_b , is

$$v_{l,b} = \left[(v_L - v_O) + (v_O - v_S) \frac{D_L}{D_S} \right]_{l,b}, \quad (9)$$

where v_L and v_S are the lens and source velocities drawn from the distribution given by eq. (8). The total transverse velocity is

$$v_t = (v_l^2 + v_b^2)^{1/2}. \quad (10)$$

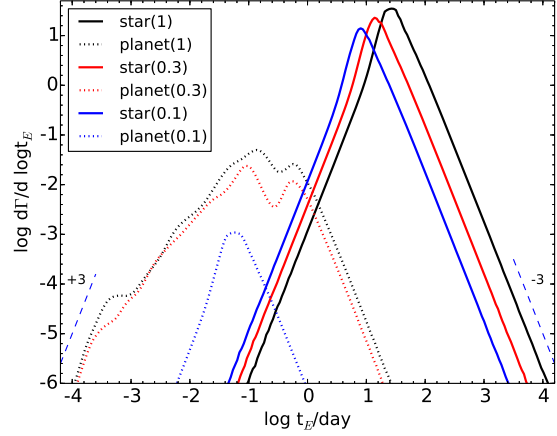


Figure 5. The event rate as a function of timescale t_E ; both axes are on logarithmic scales. The three solid curves are for the events produced by three stellar masses, 1, 0.3 and $0.1 M_\odot$, respectively. The three corresponding planetary curves (dotted lines) are shown on the left. The asymptotic slopes (Mao & Paczynski 1996) at short and long time-scales are indicated by two dashed lines.

5 RESULTS

Our main results are illustrated in Fig. 5 and also summarized in Table 2. The three curves on the right are the predicted event rates for 1, 0.3 and $0.1 M_\odot$ stars. Both the time-scale and the event rate scale as $M^{1/2}$ (a linear shift on the log-log plot). The event rate is about 14.0, 7.7 and 4.4 per million stars per year (see also Han & Gould 1996; Wood & Mao 2005; Awiphan, Kerins & Robin 2015).

The corresponding curves for the free-floating populations are shown on the left. We notice that for the 0.3 and $1 M_\odot$ curves, there are two distinct peaks at around 0.1 and 1 day, respectively, these reflect the super-Earth and the Jupiter-mass populations shown on Fig. 1; the extended tails are primarily due to very low mass planets down to $10^{-5} M_\oplus$. As expected, all the curves eventually follow the asymptotic behaviours at the very short and very long time-scales (Mao & Paczynski 1996).

Since typical lenses are predicted to be around $0.3 M_\odot$, we compare the predicted distributions for this mass with the results of Sumi et al. (2011). The event rate for FFPs is found to be $\sim 1.8 \times 10^{-3}$ times that for the stellar population and the median time-scale is shorter by a factor of ~ 16 than that for stars. If we focus on the FFPs, we find their median time-scale is much shorter ~ 0.1 days than the peak of ~ 1.6 days in Sumi et al. (2011) (see their Fig. 2). In addition, the predicted event rate for FFPs is about ~ 13 times lower than those found in the MOA data. Thus there is a serious discrepancy between observations and theory, a point we will return to in the next section.

6 SUMMARY AND DISCUSSION

In this paper, we have used the FFP population in the core accretion theory of Ida, Lin & Nagasawa (2013) to make predictions for the microlensing event rate and typical time-scale. This is accomplished with a simple Galactic model in

Table 2. The predicted optical depth τ , event rate (per million stars per year), Γ , and the mean and median (last column) time-scales in days for the stars and planets respectively. The bar angle is 30° .

		τ	Γ	$\langle \log(t_E) \rangle$	$\log t_{E,\text{med}}$
0.1 M_\odot	planet	1.4×10^{-13}	5.0×10^{-4}	-1.2	-1.3
	star	1.8×10^{-7}	4.4	0.9	0.9
0.3 M_\odot	planet	1.2×10^{-11}	1.4×10^{-2}	-1.0	-1.0
	star	5.4×10^{-7}	7.7	1.2	1.1
1 M_\odot	planet	4.4×10^{-11}	3.9×10^{-2}	-0.9	-0.9
	star	1.8×10^{-6}	14.0	1.4	1.4

terms of density and kinematics. This model has limitations, for example the mass function is not realistic. As a result, the time-scale distribution is somewhat narrower than the observed one, and our median time-scale (12.6 days) for $0.3M_\odot$ is shorter than the one with more realistic mass functions (19.2 days, Wood & Mao 2005).

We have to emphasise that the FFPs we used here are completely ejected from their systems. However, the microlensing effects of planets on wide-separation orbits may be similar to FFPs. We therefore check planets that are away from their host stars at least 3 times the Einstein radius; their typical separations are 9.6, 5.2, 3.1AU for 1, 0.3 and $0.1M_\odot$ systems respectively. Indeed, a number of wide-separation planets will be included, whose masses mostly concentrate around $100M_\oplus$. We restrict the events whose time scales are larger than 0.1 days. We find their event rates are relatively small. For example, for the $1M_\odot$ and $0.3M_\odot$ systems, the event rates are both of the order of 1.8×10^{-3} per million stars per year (these should be compared with the numbers in Table 2, 3.9×10^{-2} and 1.4×10^{-2} per million stars per year). For the $0.1M_\odot$ host star, there are no objects beyond three Einstein radii. So the inclusion of planets on wide-separations does not change our results significantly.

Our main result (shown in Fig. 5) is that the predicted time-scale is about a factor of ~ 16 shorter than the typical short time-scale events seen by the MOA collaboration (Sumi et al. 2011) while the event rate is smaller by a factor of ~ 13 . It is important to emphasise that even with this predicted low rate, the FFP population can still in principle be probed by observations, provided that the cadence is sufficiently high. The cadence requirement is already satisfied for some fields of MOA-II and OGLE-IV, and for most fields of the KMTNet that will have a cadence of 10 min to 15 min (see Henderson et al. 2014 for detailed predictions). A space satellite such as WFIRST or Euclid, with its superior photometric precision, will have sensitivities to Moon-mass planets (Penny et al. 2013; Spergel et al. 2015). Note, however, our study assumes perfect detection efficiency. This may not be such a bad assumption for KMTNet or WFIRST due to their high cadence. In any case, the observational results can be corrected for detection efficiency and then compared to our results. An additional simplification we made is that we ignored the finite source effect. Although this is reasonable for Jupiter mass FFPs, it is not a good assumption for planets below 1-10 M_\oplus , and their detectability will be reduced compared that for a point source (Bennett & Rhie 1996). So

one will need to take into account the finite source size effect and the sampling effect in order to compare our predictions and real data.

How might we resolve the apparent discrepancy between core accretion theory and observational data? One possibility may be that observations by Sumi et al. (2011) have over-estimated the number of FFPs, for example, due to blending or red noise in the data (Bachelet et al. 2015). In this regard, observations by other teams of these short-duration events will be valuable. Even more importantly, unique mass determinations using a combination of the finite source size effect (Witt & Mao 1994; Gould 1994b; Nemiroff & Wickramasinghe 1994; Yoo et al. 2004) and satellite parallax (e.g., from Spitzer, Kepler, and WFIRST, Refsdal 1966; Gould 1994a; Henderson et al. 2015; Zhu & Gould 2016) will give definitive results on the nature of the short-time-scale events.

On the theoretical side, more studies are needed to account for a missing population of FFPs with masses comparable to that of Jupiter. For example, gravitational instability, a scenario not considered here, may produce a population of gas giants (Boss 2006). Indeed, near-IR observations of nearby young clusters show evidence for isolated Jupiter-mass objects (for an example, see Peña Ramírez, Béjar & Zapatero Osorio 2016), although whether they can account for the required mass is unclear (Bowler et al. 2015, see Fig. 4 in Henderson et al. 2015). Furthermore, Ida, Lin & Nagasawa (2013) only studied planets formed and ejected around single stars. It may be that planets formed in binary systems can be ejected more easily (Sutherland & Fabrycky 2015). Even in the single star scenario, the ratio of the predicted frequency of gas giants in eccentric orbits compared to that in nearly circular orbits is 5 times lower than that found in radial velocity surveys (see Ida, Lin & Nagasawa 2013 for more discussions). The underestimation in their prediction may be because the secular perturbations between gas giants were not yet fully incorporated. This may in turn lead to an underestimation of the frequency of ejections. More efficient mechanisms for the formation of Jupiter-mass FFPs or distant Neptune-mass planets also need to be further explored. Undoubtedly, a precise determination of the mass spectrum of FFPs will provide an important test of different theories of planet formation.

ACKNOWLEDGMENTS

We would like to thank Richard Long for a careful reading of the manuscript and all the participants at the 20th microlensing (2016) workshop in Paris for a stimulating meeting. This work was supported by the Strategic Priority Research Program “The Emergence of Cosmological Structures” of the Chinese Academy of Sciences Grant No. XDB09000000, and by the National Natural Science Foundation of China (NSFC) under grant number 11333003 and 11390372 (SM). Work by WZ was supported by NSF grant AST-151168.

REFERENCES

Awiphan S., Kerins E., Robin A., 2015, ArXiv e-prints

- Bachelet E. et al., 2015, *ApJ*, 812, 136
Bennett D. P., Rhie S. H., 1996, *ApJ*, 472, 660
Bond I. A. et al., 2001, *MNRAS*, 327, 868
Boss A. P., 2006, *ApJ*, 643, 501
Bowler B. P., Liu M. C., Shkolnik E. L., Tamura M., 2015, *ApJS*, 216, 7
Cao L., Mao S., Nataf D., Rattenbury N. J., Gould A., 2013, *MNRAS*, 434, 595
Dwek E. et al., 1995, *ApJ*, 445, 716
Gaudi B. S., 2012, *ARA&A*, 50, 411
Gould A., 1994a, *ApJ*, 421, L75
Gould A., 1994b, *ApJ*, 421, L71
Gould A., Loeb A., 1992, *ApJ*, 396, 104
Han C., Gould A., 1996, *ApJ*, 467, 540
Henderson C. B., Gaudi B. S., Han C., Skowron J., Penny M. T., Nataf D., Gould A. P., 2014, *ApJ*, 794, 52
Henderson C. B. et al., 2015, *ArXiv e-prints*
Ida S., Lin D. N. C., 2004, *ApJ*, 604, 388
Ida S., Lin D. N. C., Nagasawa M., 2013, *ApJ*, 775, 42
Kim S.-L. et al., 2016, *Journal of Korean Astronomical Society*, 49, 37
Kiraga M., Paczynski B., 1994, *ApJ*, 430, L101
Mao S., 2012, *Research in Astronomy and Astrophysics*, 12, 947
Mao S., Paczynski B., 1991, *ApJ*, 374, L37
Mao S., Paczynski B., 1996, *ApJ*, 473, 57
Mordasini C., Alibert Y., Benz W., 2009, *A&A*, 501, 1139
Mordasini C., Alibert Y., Benz W., Naef D., 2009, *A&A*, 501, 1161
Nemiroff R. J., Wickramasinghe W. A. D. T., 1994, *ApJ*, 424, L21
Paczynski B., 1996, *ARA&A*, 34, 419
Peña Ramírez K., Béjar V. J. S., Zapatero Osorio M. R., 2016, *A&A*, 586, A157
Penny M. T. et al., 2013, *MNRAS*, 434, 2
Pfyffer S., Alibert Y., Benz W., Swoboda D., 2015, *A&A*, 579, A37
Refsdal S., 1966, *MNRAS*, 134, 315
Spergel D. et al., 2015, *ArXiv e-prints*
Sumi T. et al., 2003, *ApJ*, 591, 204
Sumi T. et al., 2011, *Nature*, 473, 349
Sutherland A. P., Fabrycky D. C., 2015, *ArXiv e-prints*
Udalski A., Szymański M. K., Szymański G., 2015, *Acta Astronomica*, 65, 1
Wegg C., Gerhard O., 2013, *MNRAS*, 435, 1874
Witt H. J., Mao S., 1994, *ApJ*, 429, 66
Wood A., Mao S., 2005, *MNRAS*, 362, 945
Yoo J. et al., 2004, *ApJ*, 603, 139
Zhu W., Gould A., 2016, *JKAS* in press